The Relationship between Nanoscale Architecture and Function in Photovoltaic Multichromophoric Arrays as Visualized by Kelvin Probe Force Microscopy

Vincenzo Palermo,[†] Matthijs B. J. Otten,[‡] Andrea Liscio,[†] Erik Schwartz,[‡]
Pieter A. J. de Witte,[‡] Maria Angela Castriciano,[§] Martijn M. Wienk,[‖] Fabian Nolde,[⊥]
Giovanna De Luca,[†] Jeroen J. L. M. Cornelissen,[‡] René A. J. Janssen,[‖]
Klaus Müllen,[⊥] Alan E. Rowan,*,[‡] Roeland J. M. Nolte,[‡] and Paolo Samorì*,[†,#]

*Istituto per la Sintesi Organica e la Fotoreattività, Consiglio Nazionale delle Ricerche,
Via Gobetti 101, I-40129 Bologna, Italy, Institute for Molecules and Materials, Radboud
University Nijmegen, Toernooiveld 1, 6525 ED Nijmegen, The Netherlands, Istituto per lo Studio
dei Materiali Nanostrutturati ISMN-CNR, Salita Sperone 31, 98166 Vill. S. Agata, Messina, Italy,
Laboratory of Macromolecular and Organic Chemistry, TU Eindhoven, P.O. Box 513,
5600 MB Eindhoven, The Netherlands, Max-Planck Institute for Polymer Research,
Ackermannweg 10, 55124 Mainz, Germany, and Nanochemistry Laboratory, ISIS, Université
Louis Pasteur and CNRS (UMR 7006), 8 allée Gaspard Monge, F-67000 Strasbourg, France*

Received June 4, 2008; E-mail: a.rowan@science.ru.nl; samori@isis-ulp.org

Abstract: The physicochemical properties of organic (multi)component films for optoelectronic applications depend on both the mesoscopic and nanoscale architectures within the semiconducting material. Two main classes of semiconducting materials are commonly used: polymers and (liquid) crystals of small aromatic molecules. Whereas polymers (e.g., polyphenylenevinylenes and polythiophenes) are easy to process in solution in thin and uniform layers, small molecules can form highly defined (liquid) crystals featuring high charge mobilities. Herein, we combine the two material types by employing structurally well-defined polyisocyanopeptide polymers as scaffolds to precisely arrange thousands of electron-accepting molecules, namely, perylenebis(dicarboximides) (PDIs), in defined chromophoric wires with lengths of hundreds of nanometers. The polymer backbone enforces high control over the spatial location of PDI dyes, favoring both enhanced exciton and charge transfer. When blended with an electron-donor system such as regioregular poly(3-hexylthiophene), this polymeric PDI shows a relative improvement in charge generation and diffusion with respect to monomeric, aggregated PDI. In order to correlate this enhanced behavior with respect to the architecture, atomic force microscopy investigations on the mixtures were carried out. These studies revealed that the two polymers form interpenetrated bundles having a nanophase-segregated character and featuring a high density of contact points between the two different phases. In order to visualize the relationship between the architecture and the photovoltaic efficiency, Kelvin probe force microscopy measurements were carried out on submonolayer-thick films. This technique allowed for the first time the direct visualization of the photovoltaic activity occurring in such a nanoscale phase-segregated ultrathin film with true nanoscale spatial resolution, thus making possible a study of the correlation between function and architecture with nanoscale resolution.

Introduction

In a world of increasing demand for energy and a declining reserve of conventional energy resources, it is of pivotal importance to find and develop new sources of energy supply, such as solar energy.[1] Among the different kinds of photovoltaic devices, organic solar cells have the advantage of being inexpensive and easily processable, but their power conversion, which at present reaches up to 6.5%,[2] remains low compared to their silicon counterparts. The use of bulk heterojunction (BHJ) solar cells, in which the electron-donor and electron-acceptor materials are mixed in order to allow maximal charge separation, represented a breakthrough in the field.[3,4] In this type of solar cell, the high contact area between the two materials enhances the ability of photogenerated excitons to effectively reach the interface between the acceptor and the donor; ideally, the interpenetration length should be on a scale

---

[†] Istituto per la Sintesi Organica e la Fotoreattività.
[‡] Radboud University Nijmegen.
[§] Stituto per lo Studio dei Materiali Nanostrutttrati.
[‖] TU Eindhoven.
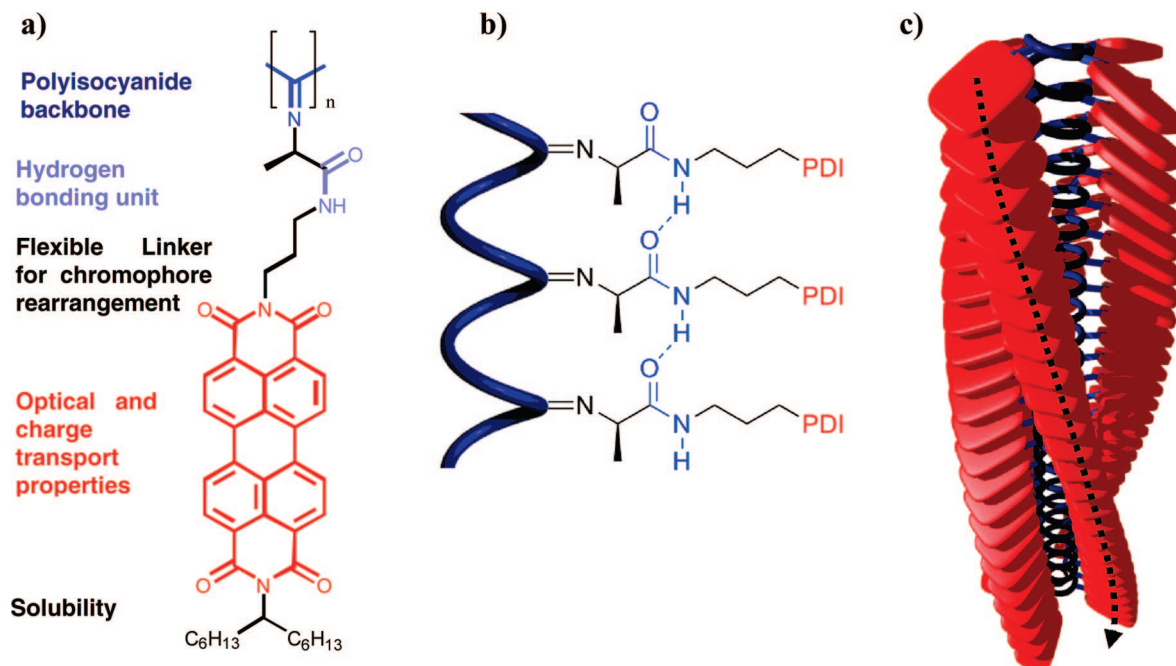[⊥] Max-Planck Institute for Polymer Research.
[#] Université Louis Pasteur.

(1) Armaroli, N.; Balzani, V. *Angew. Chem., Int. Ed.* **2007**, *46*, 52–66.

(2) Kim, J. Y.; Lee, K.; Coates, N. E.; Moses, D.; Nguyen, T. Q.; Dante, M.; Heeger, A. J. *Science* **2007**, *317*, 222–225.

(3) Halls, J. J. M.; Walsh, C. A.; Greenham, N. C.; Marseglia, E. A.; Friend, R. H.; Moratti, S. C.; Holmes, A. B. *Nature* **1995**, *376*, 498–500.

(4) Yu, G.; Gao, J.; Hummelen, J. C.; Wudl, F.; Heeger, A. J. *Science* **1995**, *270*, 1789–1791.

Figure 1. Chemical structures. (a) Chemical structure of P-PDI. The relevant parts of the molecule and their roles in the macromolecular properties are shown in different colors. (b) Illustration of the hydrogen bonding between the *n*th and (*n* + 4)th monomeric units within the polymer. The blue helix represents the carbon backbone. (c) Cartoon showing the complete helical structure of P-PDI. The dashed arrow indicates a stack of PDI units running along the central polyisocyanide backbone.

comparable to the mean exciton diffusion length, which is typically on the order of 5−6 nm.[5] Moreover, the structures within the active layer need to provide efficient pathways for the photogenerated charges to migrate to the corresponding electrodes, thereby promoting charge transport over charge recombination. Thus, the "ideal" blend for BHJ solar cells needs to feature the following well-defined characteristics: (i) The acceptor and donor materials must be interpenetrated on the nanometer scale, and hence phase separation on macroscopic scales must be hindered. (ii) The acceptor and donor materials must form continuous paths to the electrodes, and charge accumulation or recombination in dead ends and bottlenecks must be avoided. (iii) Charge transport must be efficient, with good charge mobility and a small number of defects within each phase. In the case of molecular materials, this requires good crystalline order with optimal overlap between stacked π orbitals in order to attain efficient charge-hopping transport.

Two different classes of materials are commonly employed to meet these requirements: long polymeric chains and highly crystalline assemblies of small polyaromatic molecules. While polymeric blends are easy to process and give good uniform layers, the highest charge mobilities have typically been obtained with molecular crystals of small molecules.[6] The most efficient BHJ solar cells consist of a blend of *p*-type polythiophene and *n*-type fullerene derivatives,[7−10] taking advantage of the forma-

tion of semicrystalline fullerene networks acting as percolation paths for electrons.

Polymer-based materials typically exhibit a low degree of order at the mesoscopic level because film formation is usually a kinetically governed process[11] that results in relatively low charge mobility compared with that in (liquid-)crystalline materials. On the other hand, self-assembly of small molecules is primarily thermodynamically controlled and leads to the formation of highly ordered materials. However, thermodynamically governed processes on bicomponent systems often lead to phase separation on scales larger than the exciton diffusion length. We have recently presented a novel way to overcome the polymer/small-molecule dichotomy: the use of polymeric multichromophoric arrays.[12] In these materials, small optically active molecules (chromophores) are linked to a polymeric backbone via a small peptidic spacer (an example of this class of molecules is shown in Figure 1). In this way, the chromophores have the rotational and translational freedom needed to rearrange on the molecular scale, but on a larger scale they form highly defined arrays along the polymer backbone through $\pi-\pi$ stacking and the formation of β-sheet hydrogen-bonding networks. Furthermore, the structural properties of the polymeric backbone can be controlled independently of the chromophores, giving high rigidity and ensuring the formation of efficient percolation paths into the blend. The multichromophoric array structure shown in Figure 1a was designed in order to combine five specific moieties that convey and control well-defined properties of the architecture: (i) an all-carbon polyisocyanide backbone; (ii) peptide side groups that interact through hydrogen bonding, not only inducing the backbone to adopt a 4_1 helical

(5) Scully, S. R.; McGehee, M. D. *J. Appl. Phys.* **2006**, *100*, 034907.
(6) Coropceanu, V.; Cornil, J.; da Silva, D. A.; Olivier, Y.; Silbey, R.; Brédas, J. L. *Chem. Rev.* **2007**, *107*, 926–952.
(7) Li, G.; Shrotriya, V.; Huang, J. S.; Yao, Y.; Moriarty, T.; Emery, K.; Yang, Y. *Nat. Mater.* **2005**, *4*, 864–868.
(8) Ma, W. L.; Yang, C. Y.; Gong, X.; Lee, K.; Heeger, A. J. *Adv. Funct. Mater.* **2005**, *15*, 1617–1622.
(9) Reyes-Reyes, M.; Kim, K.; Carroll, D. L. *Appl. Phys. Lett.* **2005**, *87*, 083506.
(10) Peet, J.; Kim, J. Y.; Coates, N. E.; Ma, W. L.; Moses, D.; Heeger, A. J.; Bazan, G. C. *Nat. Mater.* **2007**, *6*, 497–500.

(11) Strawhecker, K. E.; Kumar, S. K.; Douglas, J. F.; Karim, A. *Macromolecules* **2001**, *34*, 4669–4672.
(12) Hernando, J.; de Witte, P. A. J.; van Dijk, E. M. H. P.; Korterik, J.; Nolte, R. J. M.; Rowan, A. E.; Garcia-Parajo, M. F.; van Hulst, N. F. *Angew. Chem., Int. Ed.* **2004**, *43*, 4045–4049.
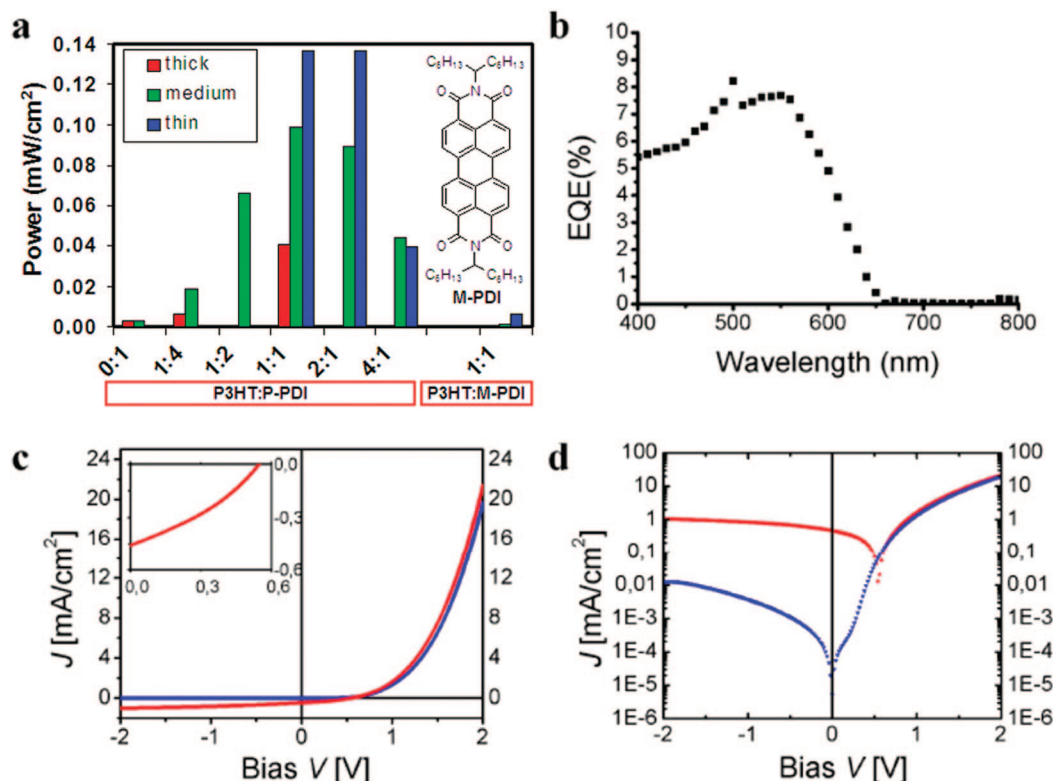
Figure 2. Performance of photovoltaic cells constructed from various blends of P3HT and P-PDI. (a) Power outputs of cells constructed using various P3HT/P-PDI ratios and spin-cast with various layer thicknesses. For comparison, results for a blend of P3HT and dihexylheptylperylenebis(dicarboximide) (labeled as M-PDI) are also given. (b) Action spectrum of a thin 1:1 P3HT/P-PDI cell. (c) Linear $J-V$ plots in darkness (blue line) and under illumination (red line) for a medium 1:1 P3HT/P-PDI cell. The inset shows a zoom-in view of the fourth quadrant. (d) Semilogarithmic $J-V$ plot of the data points in (c).

conformation (four repeats per turn) but also providing greater rigidity to the polymer;[13] (iii) a flexible linker that forces the chromophores to remain close to the polymeric chain but at the same time allows them to move, rotate, and interact on a molecular scale to maximize their $\pi-\pi$ interactions; (iv) the chromophore that provides electronic and optical function to the architecture; and (v) the alkyl side chains, which offer increased solubility in organic solvents. The combination of these moieties leads to a macromolecular system featuring high rigidity, good processability, and the capacity to generate and transport charges through $\pi-\pi$ interactions, as described below.

In this work, we have focused our attention on the nanoscale structural architecture and electronic properties of perylenebis(dicarboximide) (PDI)-functionalized polyisocyanide (P-PDI)-based blends (Figure 1) for photovoltaics. This work intentionally was not aimed at using a high-performing photovoltaic blend. Instead, its purpose was to explore the roles of architecture and chromophore–chromophore interactions within the acceptor component of the blend through a comparison of the photovoltaic activities (as determined by new force-microscopy techniques) of blends of a regioregular poly(3-hexylthiophene) (P3HT) with monomeric PDI (M-PDI) and with P-PDI.

PDI was used as the chromophore because it has been widely studied and employed in organic electronics in view of its high electron affinity, stability, and charge mobility, as measured in

both crystals and liquid crystals.[14–16] In a previous work, BHJ solar cells based on PDI with hexa-*peri*-hexabenzocoronene as a *p*-type material exhibited high external quantum efficiencies.[17] In these cells, a key role is played by the PDI nanocrystals in spanning the distance between the two electrodes, thereby allowing efficient electron transport. The best power conversion efficiency for a BHJ solar cell incorporating PDIs was reported using PDI as the *n*-type material and poly(2,7-carbazole) as the *p*-type material.[18] In all of these studies, the PDI formed large, mesoscopic aggregates within the BHJ film.

In order to initially study the effect of morphology on photovoltaic efficiency, photovoltaic devices were prepared by spin-coating a mixture of either P-PDI or M-PDI as the *n*-type material and P3HT as the *p*-type material on an indium tin oxide (ITO)/polyethylenedioxythiophene:polystyrenesulfonate (PEDOT:PSS) electrode and then depositing a top electrode of lithium fluoride (1 nm) and aluminum (100 nm).[19] A comparison of the power outputs for different cell thicknesses is shown in Figure 2. The best performance was obtained for a thin cell

(13) Samorì, P.; Ecker, C.; Gossl, I.; de Witte, P. A. J.; Cornelissen, J. J. L. M.; Metselaar, G. A.; Otten, M. B. J.; Rowan, A. E.; Nolte, R. J. M.; Rabe, J. P. *Macromolecules* **2002**, *35*, 5290–5294.

(14) Dimitrakopoulos, C. D.; Malenfant, P. R. L. *Adv. Mater.* **2002**, *14*, 99–117.

(15) Gregg, B. A.; Sprague, J.; Peterson, M. W. *J. Phys. Chem. B* **1997**, *101*, 5362–5369.

(16) Struijk, C. W.; Sieval, A. B.; Dakhorst, J. E. J.; van Dijk, M.; Kimkes, P.; Koehorst, R. B. M.; Donker, H.; Schaafsma, T. J.; Picken, S. J.; van de Craats, A. M.; Warman, J. M.; Zuilhof, H.; Sudholter, E. J. R. *J. Am. Chem. Soc.* **2000**, *122*, 11057–11066.

(17) Schmidt-Mende, L.; Fechtenkotter, A.; Müllen, K.; Moons, E.; Friend, R. H.; MacKenzie, J. D. *Science* **2001**, *293*, 1119–1122.

(18) Li, J. L.; Dierschke, F.; Wu, J. S.; Grimsdale, A. C.; Müllen, K. *J. Mater. Chem.* **2006**, *16*, 96–100.

(19) Otten, M. B. J.; Schwartz, E.; De Witte, P. A. J.; Cornelissen, J. J. L. M.; Wienk, M. M.; Janssen, R. A. J.; Nolte, R. J. M.; Rowan, A. E. *Abstr. Pap.—Am. Chem. Soc.* **2006**, *231*, PMSE 440.
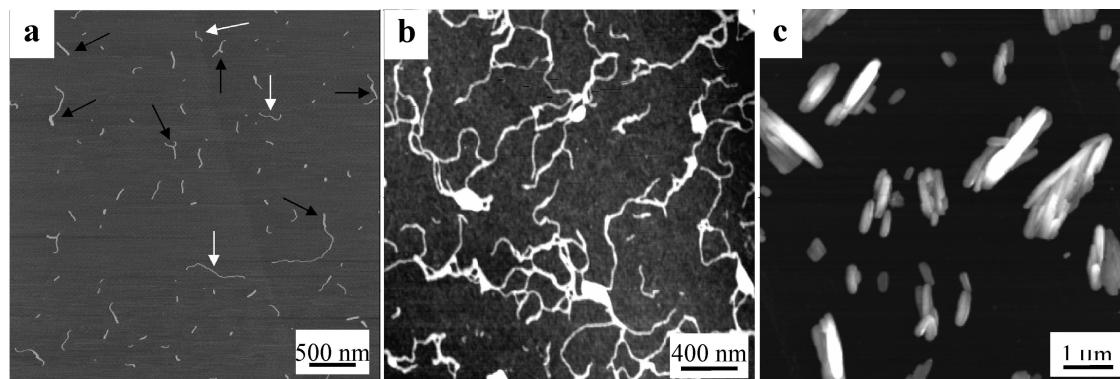
Figure 3. AFM studies of P-PDI and M-PDI. (a) Insulated strands of P-PDI on mica. (b) Network of P-PDI on SiO_x. (c) Mesoscopic crystals of M-PDI on SiO_x. Z ranges: (a) 10, (b) 8, and (c) 100 nm.

with a 1:1 ratio of the two materials, which gave an external quantum efficiency (EQE) of 8.2% at 500 nm (see Figure 2b−d for an action spectrum and J−V plots for this cell). Although this device provided a modest overall efficiency of ∼0.2%, which is far from the state-of-the-art for organic solar cells, it was noticeable that there was a 20-fold efficiency improvement for the thin cell when the P-PDI was used instead of the M-PDI. The essence of the present study is the correlation between this efficiency increase and the device and material architecture. Higher efficiencies for similar PDI monomers and P3HT have been reported, although to obtain these results, a considerably higher PDI content was needed.[20]

The relative improvement in efficiency obtained using the PDI multichromophoric wires is probably due to the interplay of several factors. First, the polymeric backbone may hinder the formation of mesoscopic PDI crystals of the type commonly observed in self-assembled PDI architectures,[17,21] and as a result, the interpenetration of P-PDI and P3HT, which is favorable for efficient charge separation between the donor and acceptor, can be increased. Second, the linear structure of the PDI wires is expected to preserve the percolation continuity of the electron-accepting phase, forming a continuous network and thus decreasing the presence of dead ends and bottlenecks.

Recently, Kelvin probe force microscopy[22] (KPFM), also known as scanning Kelvin probe microscopy (SKPM), has been extensively employed to characterize organic transistors[23] and solar cells.[24−27] KPFM is a contactless technique that allows the quantitative measurement of the electric surface potential (SP) with nanoscale resolution without significantly perturbing the potential of the system under study, thereby making possible an in situ exploration of the operation of electronic devices. The SP of a sample can to a first approximation be considered as the work function of the sample by taking into account effects due to the surface polarizability as well as band bending.

The goal of the research described below was to study more closely the origin of the increased photocurrent in devices containing P-PDI polymer compared with those incorporating M-PDI. To this end, we present an "architecture versus function" study of simple donor−acceptor blends having PDI (in either in its "classical" monomeric form or the polymeric form) as the electron acceptor and P3HT as the electron donor. Ultrathin layers of both P-PDI/P3HT and M-PDI/P3HT blends have been studied using KPFM, allowing the observation of the differences

in photogeneration of charges and potential buildup for the two different PDI morphologies with nanoscale spatial resolution.

Results and Discussion

Structural Characterization. The structural properties of P-PDI have previously been characterized by several spectroscopic techniques.[12,19,28] Absorption spectroscopy measurements on P-PDI solutions revealed the presence of strong absorption bands in the region 400−600 nm for the S_0−S_1 transition. A blue shift of the absorption maximum with respect to that of the monomer precursor was detected, which is reminiscent of exciton-coupled PDIs in a face-to-face geometry. In line with this geometry, an excimer-like fluorescence was observed,[29,30] indicating strong π−π interactions along the PDI stacks.

The resulting polymers are extremely stiff, and in atomic force microscopy (AFM) images (Figure 3a), their rigidities appeared to be higher than those of other methyl ester-substituted polyisocyanopeptides, having a persistence length over 76 nm.[13] AFM images of P-PDI spin-coated on mica from chloroform solutions (Figure 3a) showed the coexistence of fibers exhibiting a single-molecule cross section (indicated by white arrows) and their aggregates (marked with black arrows). The latter include both intersections between two chains and segments consisting of two chains tightly packed on top of each other. The limits in the spatial resolution of the AFM due to the tip convolution did not permit the determination of a distinction between these two assemblies. Analysis of the single fibers revealed a height of 1.5 ± 0.5 nm and a length of 180 ± 130 nm. More details on the statistical analysis of the polymer dimensions by AFM and light-scattering measurements are given in the Supporting

(20) Shin, W. S.; Jeong, H. H.; Kim, M. K.; Jin, S. H.; Kim, M. R.; Lee, J. K.; Lee, J. W.; Gal, Y. S. *J. Mater. Chem.* **2006**, *16*, 384–390.
(21) Palermo, V.; Liscio, A.; Gentilini, D.; Nolde, F.; Müllen, K.; Samorì, P. *Small* **2007**, *3*, 161–167.
(22) Palermo, V.; Palma, M.; Samorì, P. *Adv. Mater.* **2006**, *18*, 145–164.
(23) Burgi, L.; Sirringhaus, H.; Friend, R. H. *Appl. Phys. Lett.* **2002**, *80*, 2913–2915.
(24) Chiesa, M.; Burgi, L.; Kim, J. S.; Shikler, R.; Friend, R. H.; Sirringhaus, H. *Nano Lett.* **2005**, *5*, 559–563.
(25) Coffey, D. C.; Ginger, D. S. *Nat. Mater.* **2006**, *5*, 735–740.
(26) Hoppe, H.; Glatzel, T.; Niggemann, M.; Hinsch, A.; Lux-Steiner, M. C.; Sariciftci, N. S. *Nano Lett.* **2005**, *5*, 269–274.
(27) Palermo, V.; Ridolfi, G.; Talarico, A. M.; Favaretto, L.; Barbarella, G.; Camaioni, N.; Samorì, P. *Adv. Funct. Mater.* **2007**, *17*, 472–478.
(28) Otten, M. B. J.; Schwartz, E.; Palermo, V.; Liscio, A.; Samorì, P.; Nolte, R. J. M.; Rowan, A. E. In preparation, 2008.
(29) Rybtchinski, B.; Sinks, L. E.; Wasielewski, M. R. *J. Phys. Chem. A* **2004**, *108*, 7497–7505.
(30) Saigusa, H.; Lim, E. C. *Acc. Chem. Res.* **1996**, *29*, 171–178.
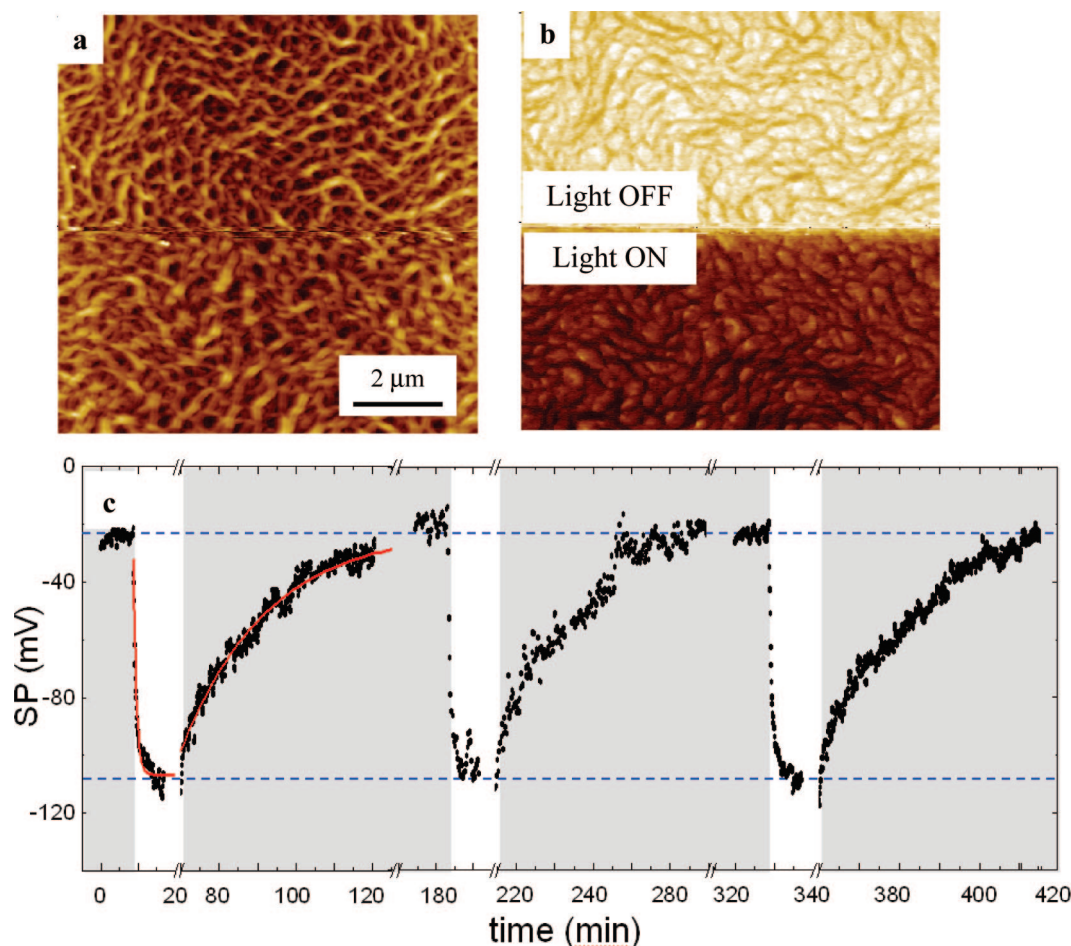
Figure 4. AFM and KPFM studies of P-PDI/P3HT films spin-coated on PEDOT:PSS. (a) Topographic image of a 60 nm thick film. (b) Corresponding KPFM image. Light was switched on during the measurement. (c) Measured SP variation for the sample under illumination with white light (60 mW cm^{-2}) (white areas) or no light (gray areas). Red lines show exponential fits of the charging and discharging processes.

Information. This type of morphology was also obtained on other substrates, such as graphite and silicon. In particular, by spin-coating a concentrated (30 mg/L) P-PDI solution onto SiO$_x$, a continuous, well-defined network of fiber bundles was obtained (Figure 3b). For the sake of comparison, M-PDI films were also prepared using similar conditions. AFM images of these films showed the presence of mesoscopic crystals (some microns long and tens of nanometers thick; see Figure 3c), pointing to a greater aggregation tendency for the monomeric compound.

By and large, the characterizations in solution and on surfaces revealed that the multichromophoric arrays exhibit different effects on different length scales. While the PDI packing is not hindered and strong $\pi-\pi$ interactions are present on a molecular level, allowing rapid exciton diffusion, on a larger scale, the aggregation of the dye molecules is hampered, with the morphology on the micron scale being dictated by the polymeric backbone, which hinders the formation of large PDI crystals.

Surface Potential of Thick Layers under Illumination. We performed AFM and KPFM measurements on bicomponent blends, such as the ones used for the preparation of real solar cells (Figure 2), but without top metallic electrode. Figure 4a shows the morphology of a 60 nm thick P-PDI/P3HT film spin-coated onto PEDOT:PSS. As expected, the morphology is quite complex: the AFM images reveal a surface consisting of intertwined yet elongated bundles of fibers with cross sections of ∼200 nm.

When illuminated with white light, the blends showed significant photovoltaic activity, with the average SP becoming more negative (darker in Figure 4b). The average potential shift, calculated for different measurements performed with different tips, amounted to 90 ± 10 mV. This negative shift of the SP has been previously observed in KPFM of photoactive blends[24−27] and can be attributed to trapping of electrons in the blend under steady-state conditions while holes can move to the underlying anode. Although a significant potential shift was observed by KPFM upon exposure to white light, no clear distinction between the two applied materials could be found: both polymers are likely to form complex three-dimensional interpenetrated networks of fiberlike structures. In this case, though, the formation of macroscopic aggregates of PDI was clearly prevented by the use of P-PDI and, in contrast to previously published results,[17,31] no micron-scale phase separation was observed.

Figure 4c displays the change in the average SP as the illumination was turned on and off. Two different regions could be distinguished in the KPFM image when turning on and off the light (the white and gray areas, respectively). During a dark/light cycle, the sample was nonilluminated for ∼100 min and then illuminated for ∼30 min. Turning on and off the light

(31) Dittmer, J. J.; Lazzaroni, R.; Leclère, P.; Moretti, P.; Granström, M.; Petritsch, K.; Marseglia, E. A.; Friend, R. H.; Brédas, J. L.; Rost, H.; Holmes, A. B. *Sol. Energy Mater. Sol. Cells* **2000**, *61*, 53–61.

caused the measured SP to switch between two asymptotic values. From fits of the measured SP trends with exponential curves (the first two curves of which are shown in red), the time constants for charge separation and recombination were calculated to be ~45 and 1500 s, respectively, revealing that the surface can remain charged for tens of minutes. These intervals are much longer than the photoinduced charge-generation ($\sim 10^{-12}$ s) and charge-collection ($\sim 10^{-6}$ s) times and hence point to the dynamics of charge trapping and detrapping (see the Supporting Information for more details). The charging/discharging dynamics on the second-to-minute scale suggest that the high, stable potential differences observed by KPFM are influenced by the presence of traps.

The experimental setup used to obtain these results required the samples to be prepared and measured in air. Thus, in order to assess whether degradation of the material due to photooxidative processes might have taken place, each sample was subjected to several dark/light cycles (Figure 4c), and the same measurements were then repeated after several days of storage in air. No significant differences were found in the measured potentials, indicating that if photooxidation was present, it had already taken place in the first minutes of exposure to air and did not influence the variations observed in the subsequent KPFM experiments. It is reasonable to expect that similar KPFM experiments performed in vacuum could exhibit even higher spatial and potential resolution also, in view of the more distinct photovoltaic activity under an inert atmosphere.

Surface Potential of Ultrathin Layers under Illumination. To gain greater insight into the process of charge separation at the nanoscale level, submonolayer-thick films of electron-acceptor/electron-donor blends were prepared using P-PDI as the electron acceptor and regioregular P3HT as the electron donor. For the sake of comparison, we extended our nanoscale-resolved study to include blends of P3HT and M-PDI, which were recently characterized by KPFM.[28] In view of the structure's thickness (a few nanometers) and lateral size (hundreds of nanometers) within the P-PDI/P3HT film, this can be considered a quasi-two-dimensional acceptor/donor blend. The structure within the film is therefore nearly flat, which is much simpler than in the case of a conventional, tens-of-nanometers-thick solar cell and, more importantly, completely accessible by the scanning probe of the microscope. As a substrate, we employed *p*-type Si(100) ($R \approx 10\ \Omega$ cm) because of its high flatness and the absence of steps or defects in areas up to the micrometer scale and, more generally, in view of its relevance in micro- and nanoelectronics. The work function (WF) of Si is ~5.0 eV,[32] which is similar to that of the PEDOT:PSS substrate typically employed for the preparation of solar cells (5.0 eV).[20] The main difference between the silicon and PEDOT:PSS substrates is the presence of a thin layer (1.5–2 nm) of native oxide on the silicon surface. Thus, the deposited nanostructures can be considered as electrically insulated from the substrate, although partial charge transfer to the substrate can take place by electron tunneling, in view of the limited oxide thickness.[33] Figure 5 shows results for ultrathin blends of P-PDI with P3HT. In the case of P-PDI, nanoscopic bundles of single-polymer chains forming a continuous network could be resolved in the topography (Figure 5a) and SP images (Figure 5c), as recorded by KPFM. Although the morphology is complex, two different kinds of structures can be observed: sparse, thick fibers (black arrow) surrounded

by a more dense network of thin fibers (white arrow). The thick fibers had an average width of 190 ± 50 nm and a height of 17 ± 3 nm. The thin fibers exhibited an average width of 70 ± 24 nm and a height of 3.5 ± 1.0 nm. Since all of the observed fibers possessed cross sections much larger than the polymer diameter, they were composed of many bundled single-polymer chains. The topography images do not offer information on the chemical composition of the observed features, yet the SP map obtained by KPFM unambiguously reveals a clear difference in contrast between the two architectures (Figure 5c). The SP of the thick fibers appears much more negative (darker in the KPFM image) than the silicon substrate, whereas the potential of the thin fibers is slightly more positive. It should be noted that SP differences between nanoscale adsorbed architectures and the substrate as measured by KPFM are usually smaller than the real ones, because the potential measured by the tip is governed by electrostatic interactions over a surface area much larger than the nanostructures. It is possible to account for and minimize the effect of these long-range interactions by using a recently developed procedure in which the measured KPFM signal is deconvoluted from the transfer function of the microscope (see the Supporting Information for more details). This procedure allows the reconstruction of the SP image of the surface using a "charge/image charge" model and the determination from this model of the true potential even of tiny nanometric structures.[34,35] Figure 5d,f displays the measured and simulated potential profiles measured in darkness and under illumination. In any case, the real SP difference is higher or, in the best case, equal to the one measured with KPFM.

The observed potential difference between the two structures (~30 mV before deconvolution), which arises from a partial charge transfer between the two materials, indicates that the thick fibers are (mostly) composed of electron-accepting P-PDI and the thin ones of electron-donating P3HT. The dimensions of the P3HT fibers are in good agreement with previous observations,[36,37] It should be noted that the morphological distribution of P3HT seems to be influenced by the presence of the thicker P-PDI fibers, with many P3HT strands adopting a stretched conformation bridging neighboring P-PDI molecules.

Figure 6a displays a topography image of a film consisting of M-PDI codeposited with P3HT. The film morphology is much less regular and more poorly resolved. Large patches of amorphous material (indicated by the label **1** in Figure 6a) are surrounded by smaller, more crystalline clusters (indicated by black and white arrows). Through an extension of the study to include neat films of both M-PDI and P3HT (see Figure S4 in the Supporting Information), it was possible to attribute the small clusters to M-PDI-rich aggregates, while P3HT forms the rough, irregular amorphous structures (labeled as **1**). Only a few M-PDI clusters are in physical contact with the P3HT. Moreover, the morphology of M-PDI when codeposited in a blend with P3HT (Figure 6) exhibits a lower crystalline character than the neat M-PDI architectures shown in Figure S4.

(32) Michaelson, H. B. *J. Appl. Phys.* **1977**, *48*, 4729–4733.

(33) Palermo, V.; Jones, D. *Mater. Sci. Eng., B* **2002**, *88*, 220–224.

(34) Liscio, A.; Palermo, V.; Gentilini, D.; Nolde, F.; Müllen, K.; Samorì, P. *Adv. Funct. Mater.* **2006**, *16*, 1407–1416.

(35) Lyuksyutov, S. F.; Paramonov, P. B.; Sharipov, R. A.; Sigalov, G. *Phys. Rev. B* **2004**, *70*, 174110.

(36) Kiriy, N.; Jahne, E.; Adler, H. J.; Schneider, M.; Kiriy, A.; Gorodyska, G.; Minko, S.; Jehnichen, D.; Simon, P.; Fokin, A. A.; Stamm, M. *Nano Lett.* **2003**, *3*, 707–712.

(37) Yang, X. N.; Loos, J.; Veenstra, S. C.; Verhees, W. J. H.; Wienk, M. M.; Kroon, J. M.; Michels, M. A. J.; Janssen, R. A. J. *Nano Lett.* **2005**, *5*, 579–583.
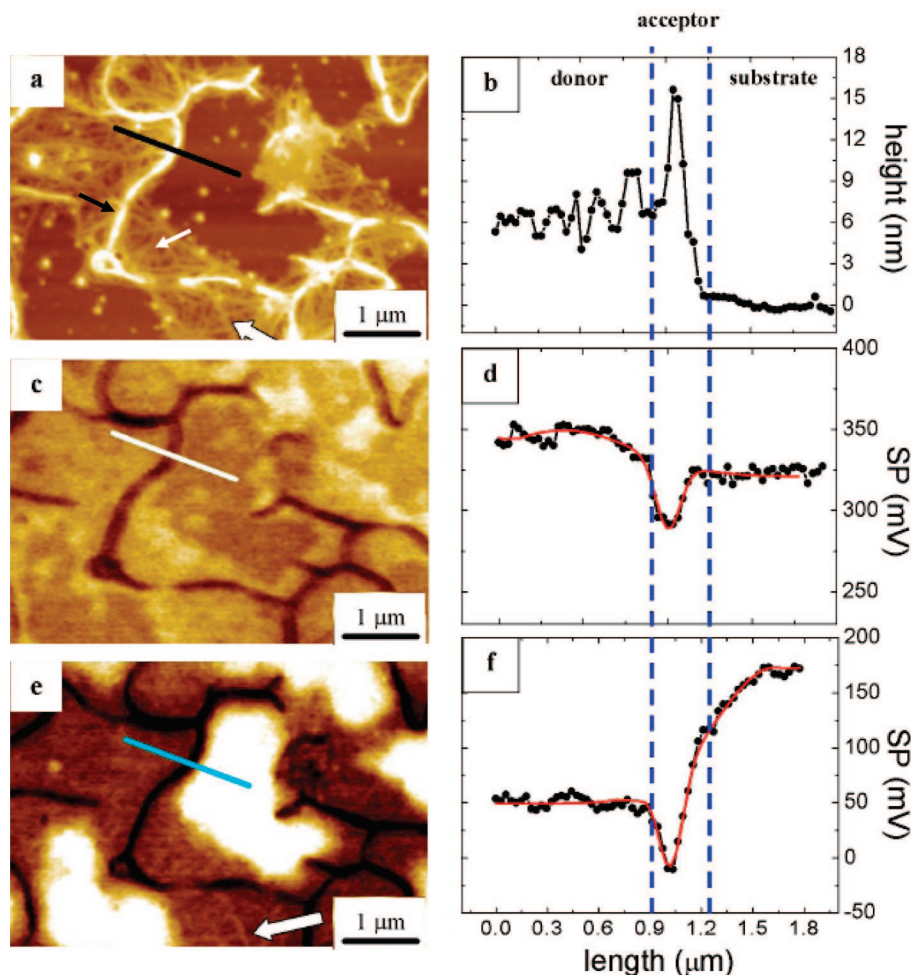
Figure 5. KPFM data on thin films of P3HT and P-PDI. (a) AFM topography image of an ultrathin blend of P-PDI and P3HT deposited on silicon. (c, e) SP images of the same area as in (a), under (c) no illumination and (e) illumination with white light ($\sim$60 mW cm^{-2}). An overall negative potential shift upon light illumination is known to occur in these types of KPFM measurements, as previously reported for thick layers (see the text); this is the reason why both PDI and P3HT appear more negative (darker) than the exposed bare silicon areas upon illumination. (b, d, f) Measured (black lines and circles) and simulated (red lines) profiles obtained by tracing the arbitrary lines in the corresponding images (a), (c), and (e). The SP values depicted are the measured ones and therefore differ from the calculated asymptotic true values reported in Table 1. Z ranges: (a) 32 nm, (c) 120 mV, and (e) 120 mV.

Table 1. Potential Differences between Donor (P3HT) and Acceptor (PDI) Phases in Blends Based on Polymeric and Monomeric PDI, Both in Darkness and under Illumination; the Change in Potential Observed in Insulated PDI Clusters (White Arrows in Figure 6a) is Also Reported[a]

|	donor/acceptor potential difference (mV)		
	P-PDI	M-PDI	insul. PDI
dark	130	10	−15
light	210	90	20
difference (light − dark)	80	80	35

[a] All of the reported values have been corrected for broadening effects due to finite KPFM tip size (see ref 36). The uncertainty of a single measurement amounts to $\sim$10 mV. The uncertainties of the SP differences can be calculated using the error propagation formula.

When the P-PDI/P3HT and M-PDI/P3HT blends were illuminated with white light, sudden changes in the surface voltage took place (Figures 5e and 6b, respectively). Significantly, an increase of the SP difference between the acceptor and donor assemblies was observed, revealing a photovoltaic effect between the PDI and P3HT aggregates. The overall surface potential becomes more negative, and the SiO$_x$ clean areas appear as positive patches with respect to the blend; both effects are due to charge transfer in the underlying substrate, as

observed in thick layers as well.[24] In the case of films of P-PDI/P3HT blends, the KPFM resolution increased notably, making it possible to resolve even the SP of single P3HT strands. Figure 5b,d,f shows the profiles obtained by tracing the arbitrary lines in the three corresponding KPFM images, along which we can distinguish both fibers (large and small) and substrate. The typical characteristic time scales for charging and discharging of the traps are several orders of magnitude smaller than the time resolution of the KPFM technique (i.e., a few milliseconds). However, the measurements were performed under steady-state conditions. During the illumination, charge generation and recombination cannot be monitored because both the deep and the shallow traps are continuously populated. Hence, the measured SP results represent an average of the charge densities, which does not show a time dependence. In contrast, when the light is turned off, the measured characteristic times are much larger than the time resolution of KPFM.

A clear and reproducible difference in the SP of such submonolayer thick films (Figure 5) was observed while turning the light on and off, showing different behaviors for charging and discharging. However, saturation of the potential on a scale of many seconds was mapped in a reproducible manner upon turning the light on and off. This suggests that the observed
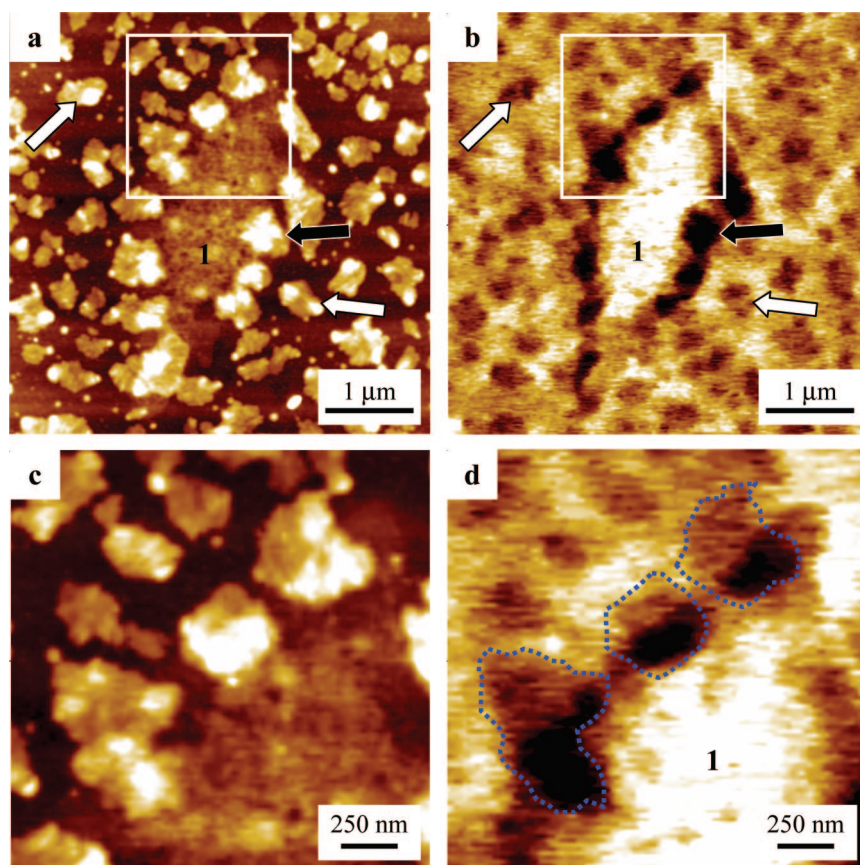
Figure 6. AFM and KPFM studies of M-PDI/P3HT blends. (a) Topographic and (b) corresponding KPFM images of a M-PDI/P3HT blend on native silicon oxide. The potential image was recorded under illumination with white light (60 mW cm^{-2}). M-PDI agglomerates are isolated (white arrows) or in contact (black arrows) with P3HT islands (marked as **1**). The regions inside the boxes in (a) and (b) are displayed at higher resolution in (c) and (d), respectively, showing in greater detail the morphology of the M-PDI agglomerates, which are marked by the dotted contours in the KPFM image. Z ranges: (a) 17 nm, (b) 63 mV, (c) 17 nm, and (d) 63 mV.

potential differences were due to charging of deep traps present in both materials by photogenerated holes and electrons. The uniform charging observed on thick and thin fibers shows that the photogenerated charges travel even tens of microns away from the visible P-PDI/P3HT interfaces.

The surface potential measured at different points on the P-PDI fibers appeared to be uniform within experimental error, indicating a uniform level of charging of the material. The AFM and KPFM results shown above indicate that when deposited in ultrathin layers, P-PDI and P3HT form architectures that are effectively phase-segregated yet interdigitated on a scale of hundreds of nanometers, with both a high contact area between the two materials and defined percolation paths for the charges.

A photovoltaic effect was also observed on M-PDI/P3HT blends,[28] but there were significant differences with the results obtained for the P-PDI/P3HT system. First, the observed potential difference between the two phases with the light off was much smaller than in the case of P-PDI. Second, the charging of the M-PDI clusters obtained upon light irradiation varied greatly. Figure 6b displays the KPFM image corresponding to the topographic image shown in Figure 6a. In particular, upon light irradiation, the PDI clusters in contact with the P3HT island (black arrows) became much more negatively charged (they appear more dark in the KPFM image) than the clusters at a larger distance from any P3HT island (white arrows). Figure 6c,d shows in greater detail the morphology and SP images, respectively, of M-PDI agglomerates in contact with P3HT. Individual aggregates are marked by dotted contours in the SP

image. The part of the cluster in connection with P3HT has a higher negative charge, while the other part of the same cluster, which is in contact with SiO$_x$, has a lower charge. This evidence indicates that the charges that are generated at the M-PDI/P3HT interface are strongly localized and do not diffuse very far from the acceptor−donor interface.

Table 1 summarizes the potential differences observed for the P-PDI/P3HT and M-PDI/P3HT blends both in darkness and under illumination. All of the reported values have been corrected for broadening effects due to the finite KPFM tip size.[34] Thin films of neat P-PDI or M-PDI adsorbed on native silicon oxide surfaces did not exhibit any change in potential upon light irradiation, whereas thin films of P3HT showed only a small, uniform (~70 mV) potential change, as can be expected as a result of the alignment of the P3HT HOMO level with the SP of the silicon substrate.[20,32]

Although the acceptor−donor potential differences (rows 1 and 2 in Table 1) observed for the P-PDI-based blend are much greater than those for the M-PDI blend, the voltage buildup upon illumination (the light−dark difference, row 3 in Table 1) is the same, indicating that the electronic properties of P-PDI are not significantly different from those of M-PDI.

Thus, in the particular case of ultrathin layers, the use of P-PDI instead of M-PDI gives a blend which features (i) a good contact area between the two phases, (ii) a continuous percolation network for both types of polymeric bundles, and (iii) good charge diffusion, even at large distances from the acceptor−donor interface. Comparison of the results obtained for M-PDI and

P-PDI in solution, thin layers, and blends permits some conclusions to be drawn. In solution, the main effect of having a polymeric backbone that bridges the PDI is that $\pi-\pi$ interactions (and hence electron migration) are more favored, leading to a blue shift in absorption and an excimer-like emission, even in very dilute conditions (see refs 12 and 19). On surfaces, the morphologies obtained with the two PDI molecules are notably different: the presence of a polymeric backbone prevents aggregation of the dyes and formation of large crystals, giving a percolated network instead of the large needles observed with M-PDI. Finally, in blends with P3HT, the morphology and self-assembly behavior of M-PDI is perturbed, yielding clusters with low crystallinity and more disordered crystals, whereas P-PDI forms well-defined networks in which the two components form bundles having different dimensions.

It is likely that the HOMO and LUMO of a single PDI chromophore in P-PDI do not differ from those of a single M-PDI because the N atoms of the imide groups are located at nodes in the π orbitals,[38,39] and thus, the aromatic core is separated from the polyisocyanide backbone by a peptide—propyl linker (Figure 1a) that does not influence the electronic structure of the PDI moiety.[40] The only difference, observed by characterization in solution,[12] is a stronger interaction between PDIs along the polymeric backbone. Although the chemical and electronic structures of the chromophores are not modified, the changes in morphology and self-assembly properties in P-PDI as compared with M-PDI lead to a considerable difference in the photovoltaic behaviors of the respective blends. Phase segregation and clustering are absent in P-PDI, and its photo-induced potential difference (as measured by KPFM) is much larger; also, in contrast to the M-PDI blends, uniform charging is obtained in each phase of the P-PDI blends over the whole surface.

Conclusion and Outlook

In summary, we have employed a polyisocyanide-based scaffold to form multichromophoric arrays of PDIs. When these electron-accepting and ultrarigid polymers were blended with an electron-donating system such as poly(3-hexylthiophene), a continuous path of nanophase-segregated yet interdigitated electron-accepting and electron-donating nanostructures was formed. Its morphological characterization was accomplished by AFM and KPFM. Most significantly, in contrast to previous KPFM studies reporting on the characterization of mesoscopic films (with a layer thickness >100 nm), which could not offer direct insight into the correlation between surface-potential variations and molecular structure, the KPFM measurements performed here show for the first time the nanoscale photovoltaic activity in polymeric bundles of electron-accepting PDI wires and bundles of electron-donating P3HT chains.

The use of rigid polymer chains as scaffolds to control the position of dyes is not limited to PDI on polyisocyanides, and a whole class of ultrastiff nanowires based on different chro-

mophores is accessible.[41] The possibility of independently tuning the mechanical properties of the polymer [i.e., the rigidity of the wire (on the nanometer scale) and the linker flexibility and dye stacking (on the molecular scale)] by chemical modification will add to the continuously growing toolbox of nanoelectronics a new class of materials with much improved mechanical and electronic properties.

The ability to obtain highly resolved and quantitative mapping of the photovoltaic activity on a nanoscale has a huge potential for gaining a greater understanding of the processes of charge separation and charge mobility in polymer chains. This is crucial for the optimization of various fundamental photophysical properties of a functional bicomponent macromolecular system and ultimately for the improvement of the performance of organic solar cells (e.g., with respect to power conversion efficiency). Ongoing research in our laboratories is directed toward the study of high-performance photovoltaic blends via the combination of scaffold materials and KPFM techniques.

Experimental Section

Photovoltaic devices were prepared by spin-coating a mixture of P-PDI (as the *n*-type material) and regioregular P3HT (as the *p*-type material) on an ITO/PEDOT:PSS electrode and then eventually depositing a top electrode of lithium fluoride (1 nm) and aluminum (100 nm).[19] P-PDI/P3HT) blends with weight ratios varying between 1/0 and 4/1 were spin-coated at different rotation speeds (1500, 2500 and 4000 rpm) from chloroform solutions, giving films with different thicknesses, designated as thin (~30 nm), medium (~60 nm), and thick (~120 nm). The current—voltage ($J-V$) characteristics of the cells were measured in darkness and under illumination with a tungsten halogen lamp. UV and IR contributions were removed by Schott GG380 and Schott KG1 filters, respectively. The final intensity of 75 mW/cm^2 generated a current density in these devices that was within ±20% of the current density under solar illumination. This was confirmed by convolution of the spectral responses with AM1.5 spectrum. For comparison, two cells in which P-PDI was replaced by M-PDI were prepared.

The thin layers were prepared by drop-casting ~10 μL of a chloroform solution containing both P-PDI (30 mg/L) and P3HT (7.5 mg/L) on silicon. On the other hand, films of M-PDI:P3HT blends were prepared in a two-step procedure starting from a 0.53 mg/mL M-PDI solution and a 7.5 mg/L P3HT solution, both in CHCl$_3$. First, a 10 μL drop of the M-PDI solution was drop-cast on SiO$_x$. After ~3 h, a 10 μL drop of the P3HT solution was applied on top of the M-PDI, and the film was left to dry in air. The blend films were prepared in atmosphere saturated with vapors of CHCl$_3$ in order to slow down solvent evaporation and improve self-assembly. The silicon substrate was cleaned prior to use with a standard RCA procedure. In the ultrathin layers used here, very low concentrations of both materials were deposited on the surfaces. The concentration of adsorbate on the surface can feature a high local compositional variability on the nanoscale, while on the scale of hundreds of nanometers it complies with the ratio of the deposited materials. This behavior is different from that of classical thick layers.

AFM/KPFM. AFM measurements on the P-PDI fibers for analysis of heights and lengths were performed with a commercial AFM apparatus (Nanoscope III, Digital Instruments). A solution of P-PDI (~10^{-6} M in CHCl$_3$) was spun (1600 rpm) onto freshly cleaved graphite or Muscovite mica. All of the images were recorded with the AFM operating in tapping mode in air at room temperature, with a resolution of 512 × 512 pixels and moderate scan rates (1—2 lines/s). Commercial tapping-mode tips (NT-MDT, NSG10) with resonance frequencies of 190—325 kHz were used.

(38) Cotlet, M.; Masuo, S.; Luo, G. B.; Hofkens, J.; Van der Auweraer, M.; Verhoeven, J.; Müllen, K.; Xie, X. L. S.; De Schryver, F. *Proc. Natl. Acad. Sci. U.S.A.* **2004**, *101*, 14343–14348.

(39) De Schryver, F. C.; Vosch, T.; Cotlet, M.; Van der Auweraer, M.; Müllen, K.; Hofkens, J. *Acc. Chem. Res.* **2005**, *38*, 514–522.

(40) Balakrishnan, K.; Datar, A.; Naddo, T.; Huang, J. L.; Oitker, R.; Yen, M.; Zhao, J. C.; Zang, L. *J. Am. Chem. Soc.* **2006**, *128*, 7390–7398.

(41) de Witte, P. A. J.; Castriciano, M.; Cornelissen, J. J. L. M.; Scolaro, L. M.; Nolte, R. J. M.; Rowan, A. E. *Chem.—Eur. J.* **2003**, *9*, 1775–1781.

In order to reduce surface contamination due to air and, in particular, water and oxygen adsorption, the scanning probe measurements were performed under an N_2 atmosphere at a relative humidity (RH) of < 10%.

Lengths and heights were evaluated using "Scanning Adventure" image-recognition software, which was developed by Jaques Barbet. For all of the values derived from AFM data presented in this paper, the error was evaluated as the standard deviation, as measured in many different measurement sessions.

Measurements combining AFM with KPFM were performed at room temperature in a sealed chamber filled with N_2 (RH < 10%) using a commercial apparatus (Veeco Multimode IIIA equipped with the Extender Electronics module). Antimony (*n*)-doped silicon tips were used. In order to obtain sufficiently large and detectable mechanical deflections, we employed soft (k < 4 N/m) cantilevers with oscillating frequencies in the range 60 kHz < ω < 100 kHz (SCM, Veeco). Both sides of the cantilever were coated with 20 nm of PtIr, using a buffer layer (3 nm) of Cr to improve the adhesion. To acquire "simultaneous" AFM and KPFM images, a topographic line scan was first obtained by AFM operating in tapping mode, and then that same line was rescanned in lift mode with the tip raised to a lift height of ∼20 nm. The basic principles of KPFM have been described in detail elsewhere.[34] In brief, KPFM provides a local measure of the SP differences between the conductive tip and the sample under investigation. The SP is defined as (WF$_{tip}$ − WF$_{sample}$ − Δ_{pol})/q, where WF$_{tip}$ and WF$_{sample}$ are the work functions of the tip and sample, respectively, Δ_{pol} is the polarization induced by the tip, and q is the magnitude of the elementary charge. In the KPFM experiments performed in this work, a bias voltage $V_{tip} = V_{DC} + V_{AC} \sin \omega t$, where ω is the resonant frequency of the cantilever and V_{DC} and V_{AC} are continuous and alternate biases, respectively, was applied directly to the tip, and the sample was held at the ground potential. A feedback loop continually adjusted V_{DC} to nullify the force component between the tip and the sample at frequency ω. V_{DC} was recorded as a function of the position, yielding a map of the sample SP. Calibration and optimization of the experimental parameters were achieved using the procedure proposed by Jacobs et al.[42]

Scanning probe microscopies are local probe techniques that reveal local features, which are not necessarily representative of the whole sample surface. Because of this, it is appropriate to record and process several images on different points of the sample surface. This makes it possible to minimize the influence of a particular sample area and to determine an average behavior. All of the evaluations were carried out quantitatively and averaged over a large number of samples. Widths measured with AFM were corrected for tip broadening.[43]

Supporting Information Available: Determination of polymer length by AFM and light scattering, AFM studies of neat thin films of M-PDI and P3HT on SiO_x, deconvolution procedures for the KPFM measurements, and optoelectronic characterization of thick P-PDI/P3HT blends. This material is available free of charge via the Internet at http://pubs.acs.org.

JA804069N

(42) Jacobs, H. O.; Leuchtmann, P.; Homan, O. J.; Stemmer, A. *J. Appl. Phys.* **1998**, *84*, 1168–1173.
(43) Samorì, P.; Francke, V.; Mangel, T.; Müllen, K.; Rabe, J. P. *Opt. Mater.* **1998**, *9*, 390–393.